

Available online at www.sciencedirect.com

ScienceDirect

journal homepage: <http://www.elsevier.com/locate/acme>

Original Research Article

Design and static testing of a compact distributed-compliance gripper based on flexure motion

Guangbo Hao^{*}, Ronan Brendan Hand

School of Engineering-Electrical and Electronic Engineering, University College Cork, Cork, Ireland

ARTICLE INFO

Article history:

Received 17 February 2016

Accepted 23 April 2016

Available online

Keywords:

Gripper

Compliant mechanisms

Distributed-compliance

Compactness

Testing

ABSTRACT

There are precision issues with traditional rigid-body grippers due to their nature in presence of joints' backlash and friction. This paper presents a macroscale compliant gripper to eliminate these issues for the applications in handling delicate/brittle materials such as powder granular or manipulating sub-millimetre objects such as optical fibre and micro-lens. The compliant gripper is obtained from a 2-PRRP (P: prismatic; R: revolute) kinematic mechanism, and uses distributed-compliance joints for avoiding stress-concentration and enabling large range of motion. A very compact design is achieved by using a position space principle. The compliant gripper is modelled, fabricated, followed by comprehensive testing for characterising relationships between the input displacement/force and output displacement and between the input displacement and displacement amplification ratio, and for analysing hysteresis during loading and unloading. The experimental results are compared with finite element analysis (FEA) model and linear analytical model. The testing results have suggested good performance characteristics of this compliant gripper such as a nearly linear relationship between the input and output, a nearly constant amplification ratio for closing the jaw, and negligible hysteresis error.

© 2016 Politechnika Wroclawska. Published by Elsevier Urban & Partner Sp. z o.o. All rights reserved.

1. Introduction

Traditional rigid-body grippers often suffer from issues of poor resolution and repeatability associated with backlash and friction inherent in their joints [1], which are thus not suitable for handling delicate/brittle materials such as powder granular or manipulating sub-millimetre objects such as optical fibre and micro-lens. Compliant mechanisms (CMs), aka flexure mechanisms, transfer and transform motion, load and energy by deformation of their flexible members (materials) [2–4], which are good candidates to remove the above mentioned

issues in traditional grippers. In addition, CMs can be easily miniaturised, can reduce the number of parts (thereby raising the system reliability) and are free of assembly by a monolithic fabrication. CM-based grippers (compliant gripper) have been successfully used in the applications of precision robotic manipulation, biomedical devices and microelectromechanical systems (MEMS) [5–15].

There are mainly two methods to design a compliant gripper: structure optimisation method [12,14,15], and kinematics-based substitution method [5–10,13]. The former design approach is to re-consider the design task as an optimal material distribution problem so that the resulting

^{*} Corresponding author. Tel.: +353 214903793.

E-mail address: G.Hao@ucc.ie (G. Hao).

<http://dx.doi.org/10.1016/j.acme.2016.04.011>

1644-9665/© 2016 Politechnika Wroclawska. Published by Elsevier Urban & Partner Sp. z o.o. All rights reserved.

structure can fulfil the specified motion requirements. The optimisation approach based design involves three aspects: (a) topology, i.e. the connectivity of material, (b) size, i.e. the cross-sectional area of each segment, and (c) geometry, i.e. the orientations of the connecting segments and locations of the junctions [12]. For example, Zhu et al. [15] conducted topology optimisation of hinge-free compliant mechanisms with multiple outputs using a level set method. However, this optimisation approach generates compliant mechanisms that can be highly sensitive to manufacture error. The latter design approach is the one that we intend to use in this paper due to the well-known simplicity and clear kinematic meaning. The general procedure to use this approach to design a gripper can be shown as follows:

- (a) Selecting a proper rigid-body kinematic mechanism with/without an input amplification mechanism;
- (b) Choosing proper compliant joints to replace traditional joints in the rigid-body kinematic mechanism;
- (c) Arranging relative positions of adjacent compliant joints if possible for most compact design;
- (d) Check if the final compliant gripper meets the design requirements. If not, repeat the above steps.

Using the kinematics-based substitution method, lumped-compliance joints (or flexure hinges) [5–10] are often chosen since they enable to directly replace their rigid-body counterparts in the traditional parallelogram mechanisms, slider-crank mechanisms, and straight-line linkages [5–10], in order to design a compliant gripper. For example, Ref. [10] reported an asymmetric flexible micro-gripper mechanism based on flexure hinges, where the parallelogram mechanism is employed to guide motion of one jaw with the input displacement amplified by a lever mechanism. However, lumped-compliance leads to limited motion range, and can cause stress-concentration issues and especially requires a large actuation force. The large actuation force is able to be offered by piezoelectric (PZT) actuators with high-precision [5–10]. The use of a PZT actuator requires pre-stressing and particularly needs a displacement amplification mechanism [5–10,16] to amplify the input displacement since the PZT actuator only produces tiny displacements. Despite the merit, the introduction of a displacement amplification mechanism adversely degrades the resolution of the actuator. Due to the hysteresis issue from the PZT actuator [17], an open-loop control is not feasible. Moreover, it is still a challenging open issue to design a very compact compliant gripper since the compliant gripper's configuration is usually limited by its rigid-body kinematic mechanism when using the lumped-compliance joints.

Based on the above advances, there is a necessity in this paper to design a new and simple macroscale compliant gripper based on the following *desired design specifications*, which enables more selections of compliant grippers in different application requirements.

- *Linear output in horizontal direction only for each jaw*: This requires an output linear guiding mechanism to connect with each jaw so that sliding motion between the gripped object and the jaw can be maximally avoided, and also an even distribution of the gripping force over the manipulated sample can be achieved.

- *One linear input only*: This is required due to the fact that most high-precision linear actuators such as voice coil (VC) actuator are linear ones and cannot tolerate transverse displacements/loads. This demands an input linear guiding mechanism to control jaws simultaneously. Usually, it is desired to have the whole gripper with smaller size in the horizontal direction and therefore the linear actuator is better to be arranged in the vertical direction.
- *Large range of motion*: This desired characteristic refers to the large motion of the jaw to accommodate the large diameter change of grasped objects, which requires the use of distributed-compliance joints/modules when designing a gripper. Distributed compliance can avoid stress-concentration as well as large actuation force. The use of distributed-compliance joints enables the use of high-precision actuators with low force but large displacement output such as a VC actuator to be selected in this paper without needing an amplification mechanism (no resolution degrading). The large range of motion requires a symmetric design to enable both jaws to move as opposed to an asymmetric design in [10]. It is noted that the use of a VC actuator also requires a symmetric design for alleviating thermal sensitivity.
- *Compactness of mechanisms*: This means that the resulting gripper should have a large ratio of motion range to the mechanism's overall dimension. It is therefore desired to consider the embedded arrangements for adjacent compliant joints. If compliant revolute joints are to be selected, these with remote rotation centres should be given priority since they may reduce the mechanism footprint significantly.

The remainder of this paper is organised as follows. Section 2 elaborates the design of a compact large-range compliant gripper followed by a linear analytical kinetostatic modelling. Fabrication, testing and result comparison and analysis are provided in Section 3. Finally, conclusions are drawn.

2. Design of a compact large-range gripper

Based on the first two design specifications mentioned above, a simple 1-DOF (degree of freedom) 2-PRRP (P: prismatic, and R: revolute) kinematic mechanism (Fig. 1) is a good solution to be used as the traditional kinematic mechanism for designing a compliant gripper. Each PRRP mechanism is a double slider mechanism [18] and it can act as a displacement amplification or reduction mechanism without assistance of other mechanisms. This PRRP mechanism is a more general representation of other motion amplification or reduction mechanisms such as the bridge-type flexure mechanism [16]. The kinematic principle and all geometrical parameters are indicated in Fig. 1. Here, θ_{R1} and θ_{R2} are the rotational angle of the two R joints, and δ_{P1} and δ_{P2} is the translational displacement of the two P joints. $\delta_{in} = \delta_{P1}$ is the input motion from the linear actuator, and $\delta_{out} = \delta_{P2}$ is the motion of each jaw, which is the output of the gripper.

In order to achieve a large range of motion, two distributed-compliance joints [2] (Fig. 2) are selected to replace the traditional P and R joints in Fig. 1 where each compliant P joint is a basic parallelogram mechanism and each compliant R joint is an isosceles trapezoidal flexure mechanism with a remote rotation centre. The two compliant P joints (or compliant R joints) are identical in the compliant gripper.

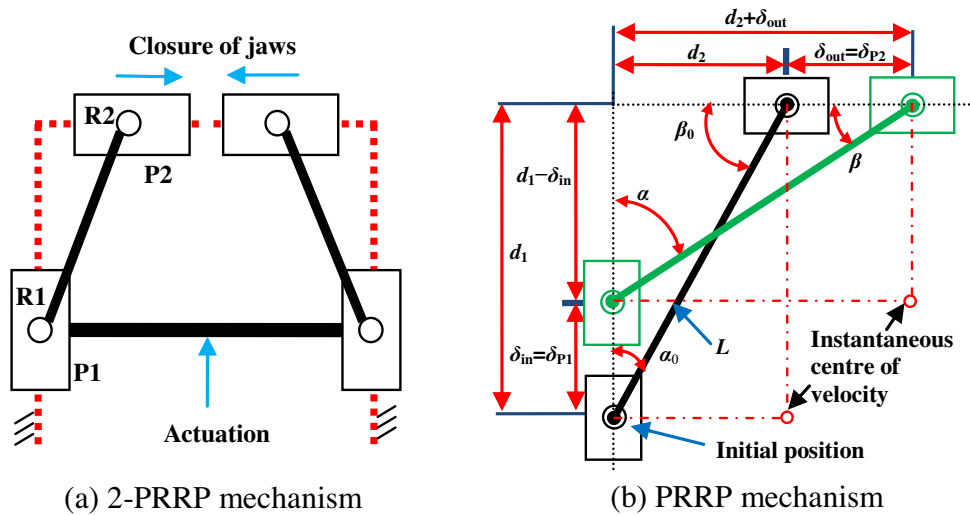


Fig. 1 - A 2-PRRP rigid-body kinematic mechanism.

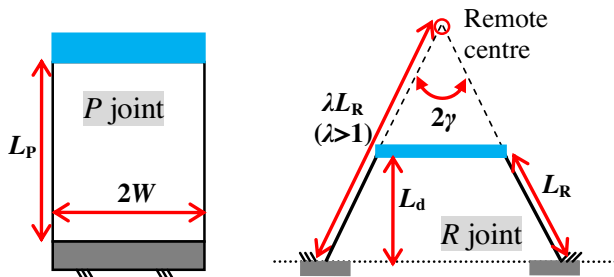


Fig. 2 - Compliant joints (all beams' in-plane thickness: T ; beam out-of-plane thickness: U ; Young's modulus: E).

Furthermore, based on the position space principle as reported in [19-21] all compliant joints can be arranged appropriately to lead to a most compact compliant gripper as shown in Fig. 3. Here, each compliant P joint can rotate about its translational direction, and each compliant R joint can rotate about its remote centre so that each PR or RP joint can be in an embedded layout (Fig. 3(a)). The position space of a compliant module is the combination of all permitted

positions in a mechanism where the constraint of this compliant module in the mechanism remains unchanged when the position of the compliant module changes relative to its adjacent compliant module rather than being considered in isolation. The position space can be identified using the screw theory [19,20], which is not only useful for gripper design but also for more general compliant mechanism design [20,21].

The linear kinetostatic model of the compliant gripper is detailed below, which is to be used to compare with the finite element analysis (FEA) model and experimental testing result in the next section.

The primary motion of each compliant joint associated with the input motion can be firstly derived based on the kinematic principle in Fig. 1 as below

$$\begin{cases} \theta_{R1} = \alpha - \alpha_0 = \arccos\left(\frac{d_1 - \delta_{in}}{L}\right) - \alpha_0 \\ \theta_{R2} = \beta_0 - \beta = \beta_0 - \arcsin\left(\frac{d_1 - \delta_{in}}{L}\right) \\ \delta_{P1} = \delta_{in} \\ \delta_{P2} = \delta_{out} = L \sin\left(\arccos\left(\frac{d_1 - \delta_{in}}{L}\right)\right) - d_2 = \sqrt{L^2 - (d_1 - \delta_{in})^2} - d_2 \end{cases} \quad (1)$$

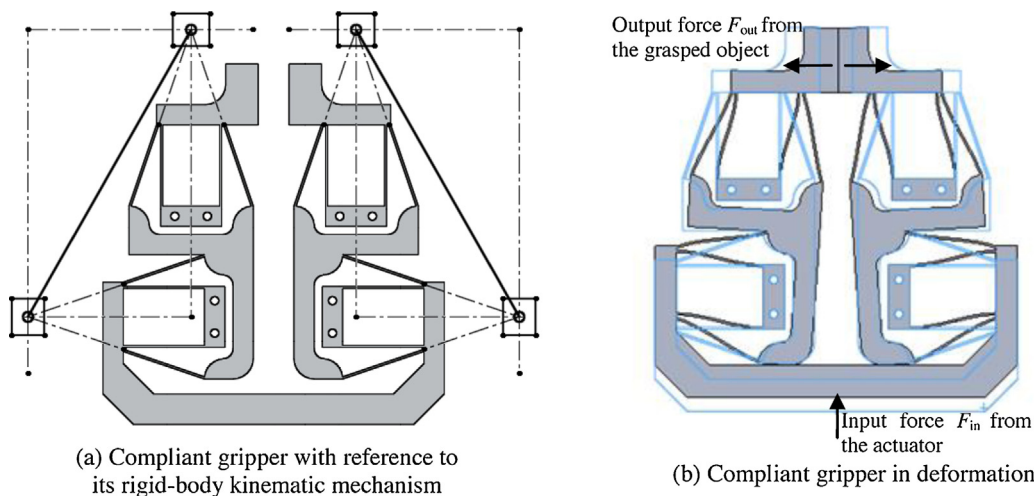


Fig. 3 - A compact large-range compliant gripper.

where all symbols are explained in Fig. 1. $\alpha_0 + \beta_0 = \alpha + \beta = \pi/2$; and $d_1^2 + d_2^2 = (d_1 - \delta_{in})^2 + (d_2 + \delta_{out})^2 = L^2$. The primary motion of each compliant joint is much smaller than the other parameters due to the nature of flexure motion. The input and output displacements are defined to be positive for closing the jaws, corresponding to the extension testing in the experiment section.

Using Eq. (1), the amplification ratio between the output displacement and the input displacement is obtained as:

$$\frac{\delta_{out}}{\delta_{in}} = \frac{\sqrt{L^2 - (d_1 - \delta_{in})^2} - \sqrt{L^2 - d_1^2}}{\delta_{in}} = \frac{\sqrt{L^2 - (d_1 - \delta_{in})^2} - d_2}{\delta_{in}} \quad (2a)$$

where if $\delta_{out}/\delta_{in} > 1$, the PRRP kinematic mechanism is a displacement amplification mechanism, otherwise, it is a displacement reduction mechanism. In this paper, a displacement amplification ratio between 1 and 2 is desired without worsening the resolution of the VC actuator too much. From Eq. (2a), it can be learnt that the amplification ratio is dependent on three independent parameters, δ_{in} , d_1 and d_2 (or L), especially on d_1 and d_2 (or L). The magnitude's increase of δ_{in} will slightly decrease the displacement amplification ratio, but the increase of d_1 will largely increase the amplification ratio, which can be seen in Fig. 4. When d_1 is very close to L , the amplification ratio is the highest.

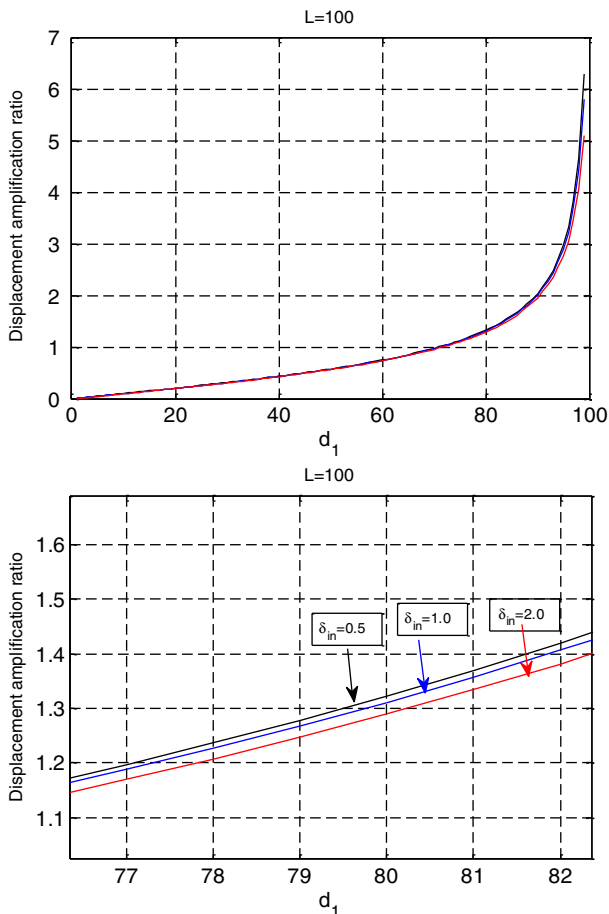


Fig. 4 – Displacement amplification ratio affected by the geometrical parameter.

The instantaneous velocity ratio between the output and the input can be derived as:

$$\frac{v_{out}}{v_{in}} = \frac{d_1 - \delta_{in}}{d_2 + \delta_{out}} = \frac{d_1 - \delta_{in}}{\sqrt{L^2 - (d_1 - \delta_{in})^2}} \quad (2b)$$

where the velocity ratio is mainly determined by the ratio of d_1/d_2 since the input and output motions are both very small.

The linear stiffness of each compliant joint (Fig. 2) that is used in this paper is further represented as follows [22,23]:

$$\begin{cases} K_{P1} = K_{P2} = 24 \frac{E(UT^3/12)}{L_p^3} \\ K_{R1} = K_{R2} = 8(3\lambda^2 - 3\lambda + 1) \frac{E(UT^3/12)}{L_R} \\ = 8(3\lambda^2 - 3\lambda + 1) \frac{E(UT^3/12)}{L_d/\cos\gamma} \end{cases} \quad (3)$$

where K_{P1} and K_{P2} are the translational stiffness of the compliant P joints, and K_{R1} and K_{R2} are the rotational stiffness of the compliant R joints. E is the Young's modulus of material. The other symbols denote the geometrical parameters as indicated in Fig. 2.

The motion range for each compliant joint can be obtained [22,23] based on the strength theory as

$$\begin{cases} \Delta_P = \frac{1}{3} \frac{\sigma_s L_p^2}{E T} \\ \Delta_R = \frac{1}{3\lambda - 1} \frac{\sigma_s L_R}{E T} \end{cases} \quad (4a)$$

where Δ_P and Δ_R are the motion range for the compliant P and R joints, respectively. σ_s is the material's yield strength. Eq. (4a) suggests that the material with larger σ_s/E and the geometry with larger ratio of beam length to beam thickness can cause larger motion range.

Therefore, for avoiding yield of material, the following conditions should be satisfied:

$$\begin{cases} \theta_{R1} < \Delta_R \\ \theta_{R2} < \Delta_R \\ \delta_{P1} < \Delta_P \\ \delta_{P2} < \Delta_P \end{cases} \quad (4b)$$

The combination of Eqs. (1) and (2) yields the potential energy of the whole gripper system due to the joints' deformation with regard to the input displacement:

$$\begin{aligned} U &= 2 \times \frac{1}{2} K_{P1} \delta_{in}^2 + 2 \times \frac{1}{2} K_{R1} \theta_{R1}^2 + 2 \times \frac{1}{2} K_{R2} \theta_{R2}^2 + 2 \times \frac{1}{2} K_{P2} \delta_{out}^2 \\ &= K_{P1} \delta_{in}^2 + K_{R1} \left[\arccos\left(\frac{d_1 - \delta_{in}}{L}\right) - \alpha_0 \right]^2 \\ &\quad + K_{R2} \left[\beta_0 - \arcsin\left(\frac{d_1 - \delta_{in}}{L}\right) \right]^2 + K_{P2} \left[\sqrt{L^2 - (d_1 - \delta_{in})^2} - d_2 \right]^2 \end{aligned} \quad (5)$$

The input force (F_{in}) in terms of an input motion (δ_{in}) incorporating the given resistance output force (F_{out}) simultaneously can be derived based on the following energy balance equation:

$$F_{in} d\delta_{in} - 2F_{out} d\delta_{out} = dU \quad (6a)$$

Substituting Eq. (5) into Eq. (6a) with the help of Eq. (1), the input force is finally obtained using the principle of virtual work [2]:

$$\begin{aligned}
 F_{in} &= \frac{dU}{d\delta_{in}} + 2F_{out} \frac{d\delta_{out}}{d\delta_{in}} \\
 &= 2K_{P1}\delta_{in} + 2K_{R1} \frac{\arccos\left(\frac{d_1-\delta_{in}}{L}\right) - \alpha_0}{\sqrt{L^2 - (d_1-\delta_{in})^2}} \\
 &\quad + 2K_{R2} \frac{\beta_0 - \arcsin\left(\frac{d_1-\delta_{in}}{L}\right)}{\sqrt{L^2 - (d_1-\delta_{in})^2}} + 2\{K_{P2}[\sqrt{L^2 - (d_1-\delta_{in})^2} - d_2] \\
 &\quad + F_{out}\} \frac{d_1-\delta_{in}}{\sqrt{L^2 - (d_1-\delta_{in})^2}} \tag{6b}
 \end{aligned}$$

The input and output forces as shown in Fig. 3 are also defined to be positive, corresponding to the extension testing in the next section. In reality, the output force F_{out} has a negligible effect since it is the very small reaction force from grasping delicate or sub-millimetre objects to produce tiny deformation. Therefore, in the following testing, the output force is not considered.

3. Testing and comparisons

In order to physically verify the performance characteristics of the proposed compliant gripper (Fig. 3), a realistic prototype was designed. The prototype geometrical sizes are determined as shown in Fig. 5 with material of AL6082 (Young's modulus $E = 69$ GPa, Poisson ratio $\nu = 0.33$ and Yield stress $\sigma_s = 276$ MPa).

This material is commonly used in precision engineering due to its good performances. A prototype was monolithically fabricated from a piece of plate using CNC milling machining and then statically tested (Fig. 6). Two displacement gauges (Digimatic Indicators, Mitutoyo Corporation, Japan) with motion resolution of 0.001 mm and a very low spring force of 0.4–0.7 N were employed to sense both input and output displacements with measurement reference points indicated in Fig. 6.

Since only CNC milling machining was available as a high-precision manufacture method for the work in this paper, the prototype was impossibly made much smaller for the same or larger range of motion. This is due to the fabrication issues associated with very small beam thickness (such as 0.4 mm), leading to the fact that the beam length could not be shorter (a slenderness ratio of 40 is used in this paper). The fabrication issues are mainly due to the nature of the contact machining that produces large loading to the flexible thin features. Even through the beam thickness is 1 mm (large enough) in our case, two supporting blocks (Fig. 7) had to be fabricated at first to be placed between beams to assist the milling machining process.

Before the static testing, finite element analysis (FEA) using Comsol was conducted to obtain simulation results to compare with the analytical model (Eq. (6b)) and testing results. The nonlinear simulation function in Comsol is activated and finest free meshing for beams is chosen. Moreover, the FEA simulation can offer a good estimation of the maximal stress to avoid material's yield so that the maximally allowable input force/displacement in testing can be determined. In our testing, the maximal input force magnitude in both loading directions is set to 80 N for

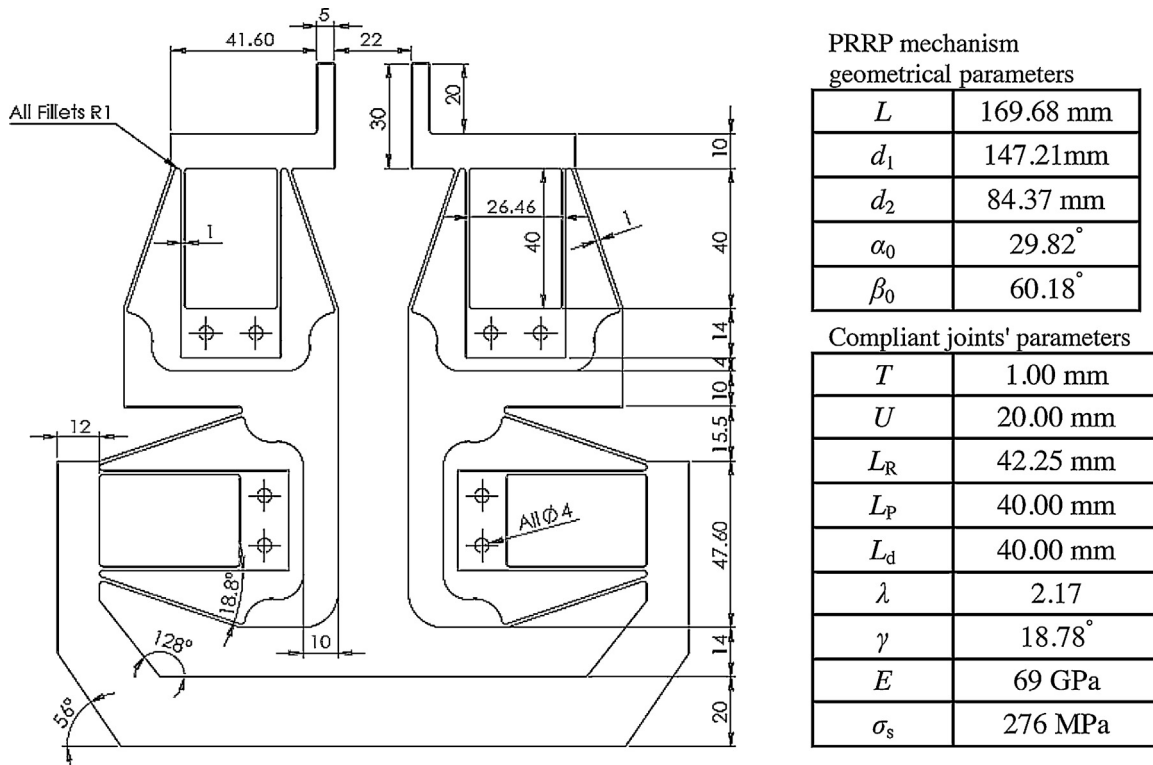


Fig. 5 – Prototype geometrical sizes (all dimensions in mm, and out-of-plane thickness 20 mm).

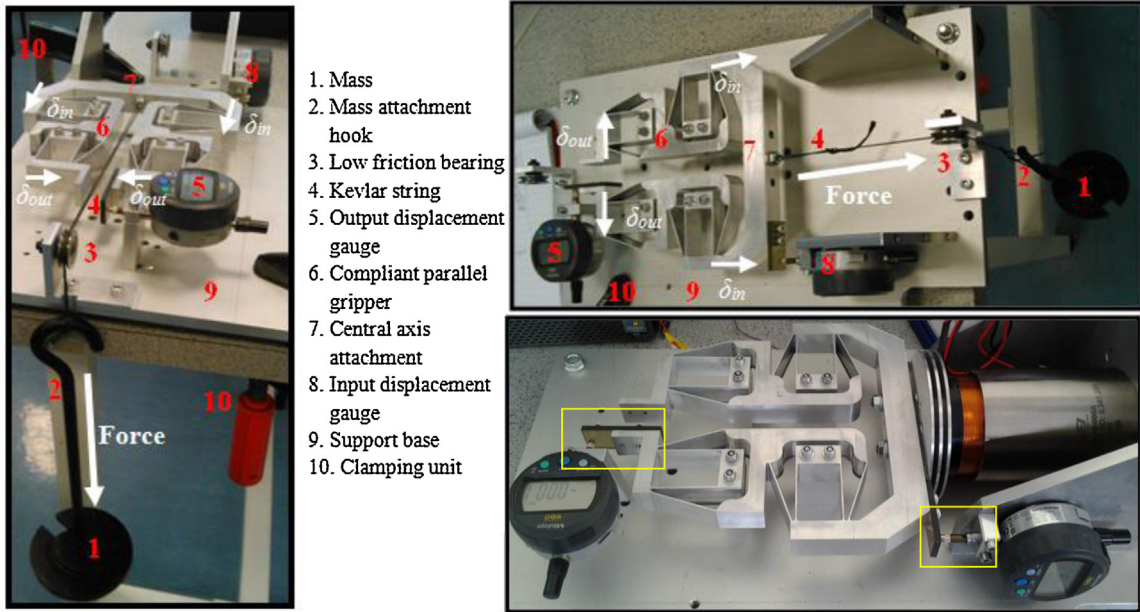


Fig. 6 – Prototype and static testing rig (left: extension testing; right top: contraction testing; right bottom: prototype with displacement gauges and a commercial VC actuator from BEI KIMCO MAGNETICS DIVISION with type number LA30-48-000A).

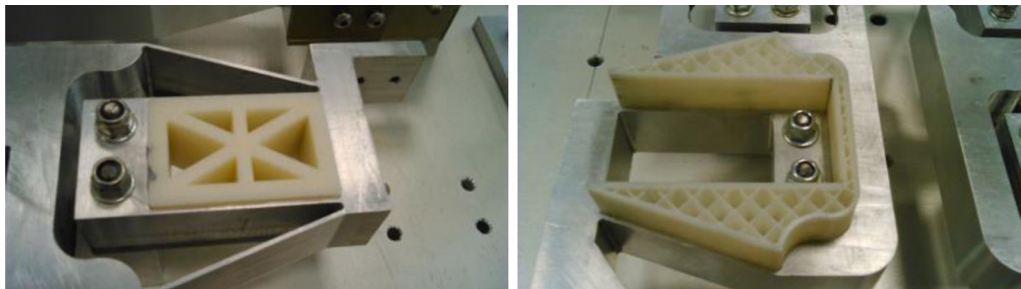


Fig. 7 – Supporting blocks for fabricating beams.

conservative loading which has been verified for not producing material's yield by both FEA and analytical model (using Eq. (4) in combination with Eqs. (6b) and (1)). Based on Eq. (6b), an 80 N input force can result in a more than ± 0.3 mm motion range for each jaw, i.e., the gripper can accommodate a diameter change of more than 1.2 mm (0.3×4) of the grasped object, which is sufficient for our applications. The initial diameter of the grasped object will decide the distance between two jaws. In our prototype, this distance is 22 mm (Fig. 5), which may be used to grip relatively large delicate object with at least a diameter of 21.4 mm and at most a diameter of 22.6 mm. If the gripper is required to grip a sub-millimetre object, two extra rectangular solid washers can be added to the two jaws to leave a very small gap between the two jaws.

The input-force and input-displacement relationship for the compliant gripper is illustrated in Fig. 8. A good correlation exists between the experimental and FEA results. The analytical model is an approximation for the gripper, but not an ideal representation of the mechanism's input displacement. For example, given a positive 50 N input force, the experimental result requires a 143 μm input displacement,

while the resulting input displacements from the analytical and FEA models are 98.9 μm (30.84% difference) and 160.1 μm (11.95% difference), respectively. The FEA model has a lower error and fits the experimental result better.

The input and output displacement relationship is additionally evaluated as illustrated in Fig. 9. The displacement

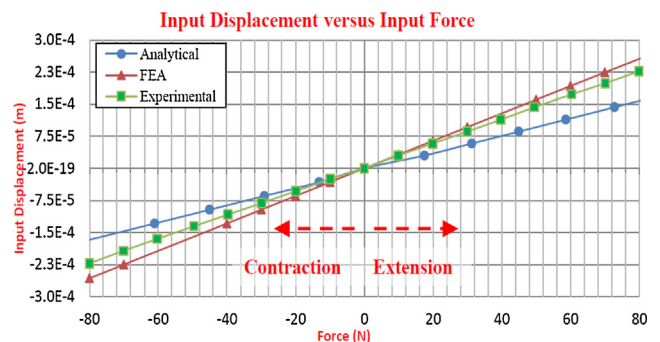


Fig. 8 – Relationship between input displacement and input force.

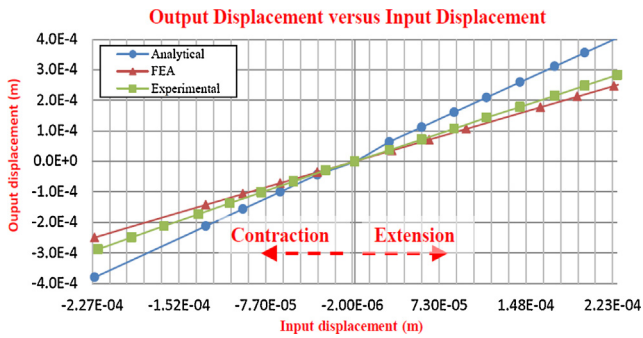
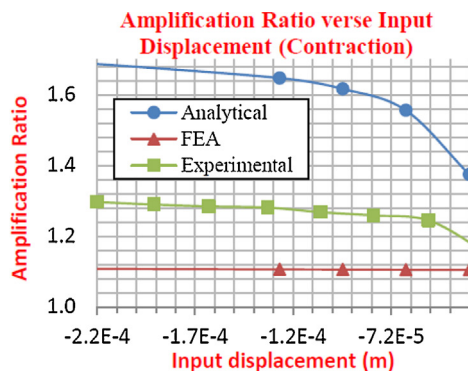


Fig. 9 – Relationship between output displacement and input force.

analysis demonstrates a good correlation between the experimental and FEA results again. The analytical model noticeably deviates from the FEA and testing results. An input displacement of $-222 \mu\text{m}$ (the input motion stage will contract and the jaws will open) defines an experimental output displacement of $-288 \mu\text{m}$. The analytical and FEA models show a $-380 \mu\text{m}$ (31.95% difference) and a $-249 \mu\text{m}$ (13.54% difference) output displacements, respectively.

The amplification ratio relates the output displacement to the input displacement. Fig. 10 illustrates the amplification ratio as a function of the input displacement. The amplification ratio changes with a change in the input displacement. Ideal constant correlations do not exist for the theoretical models and the experimental data. The contraction of the gripper defines similar trends between the analytical and experimental results where they follow the same contour at different magnitudes. The amplification ratio increases with a magnitude increase in the input displacement (negative) where the analytical and experimental values, respectively, increase by 24.1% and 11.84% from the initial value to the final value of the analysis. The FEA model does not showcase a large curvature in the plotting; instead a nearly linear relationship exists between a decreasing amplification ratio and a decreasing input displacement magnitude (0.46% decrease in the amplification through the analysis). It can be seen in the contraction case, the output displacement from the experimental results ranges from 1.16 to 1.30 times larger than the input displacement of the mechanism.



Through the extension of the mechanism the amplification ratio is nearly constant for the FEA and testing results, but the analytical results undergo a large change over the initial domain. The FEA model generates a linear relationship, with a 0.45% decrease in the amplification ratio through the increase of the input displacement. The analytical amplification ratio has an approximately exponential relationship with the input displacement, through which a 16.1% decrease occurs over the analysis. As the input displacement increases, the experimental amplification ratio initially increases up to an input displacement of $114 \mu\text{m}$ (with a 1.7% increase from 1.23 to 1.25, over the range), where the amplification ratio then slightly decreases through the remainder of the analysis. It can be observed from both the contraction and extension testing cases that the analytical model always predicts much higher amplification ratio change near the zero input displacement, which is due to the error in obtaining d_2 (for calculating amplification ratio) that only retains two digits after its decimal point.

The gripper mechanism was also tested for both loading and unloading cases to allow hysteresis observation. The mechanism is incrementally loaded and unloaded during the extension and contraction actuations. The input and output displacements are illustrated in Fig. 11(a). Fig. 11(b) illustrates the hysteresis error through the loading and unloading cycles. The maximum hysteresis errors during the mechanism's extension input displacement and output displacement are 1.76% ($4 \mu\text{m}$ difference) and 2.12% ($5 \mu\text{m}$ difference), respectively. The maximal hysteresis errors during the mechanism's contraction input displacement and output displacement are 2.31% ($6 \mu\text{m}$ difference) and 1.74% ($5 \mu\text{m}$ difference), respectively. The hysteresis error is variable during contraction and more constant during extension. The error is least during contraction for the output displacement, where some readings have no error. Fig. 11 also validates that the gripper deforms in an elastic domain only, i.e., there is no yield of material for a $\pm 80 \text{ N}$ loading.

From the above analysis, we can see that error exists between the prediction models and the experimental results. The analytical model is an ideal representation of the 2-PRR mechanism where there are no considerations of parasitic (off axis motion) effects of compliant joints, deformation of ideal rigid bodies, and primary stiffness change of compliant joints with complex loading. However, the FEA results have good agreement with the experimental ones where no ideal rigid-

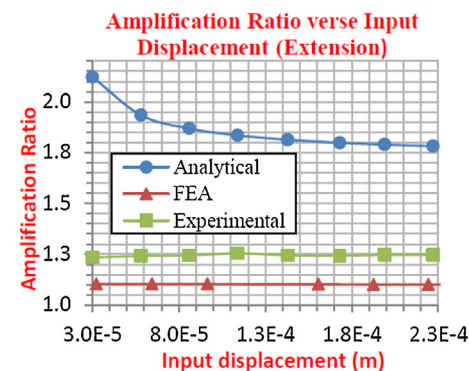
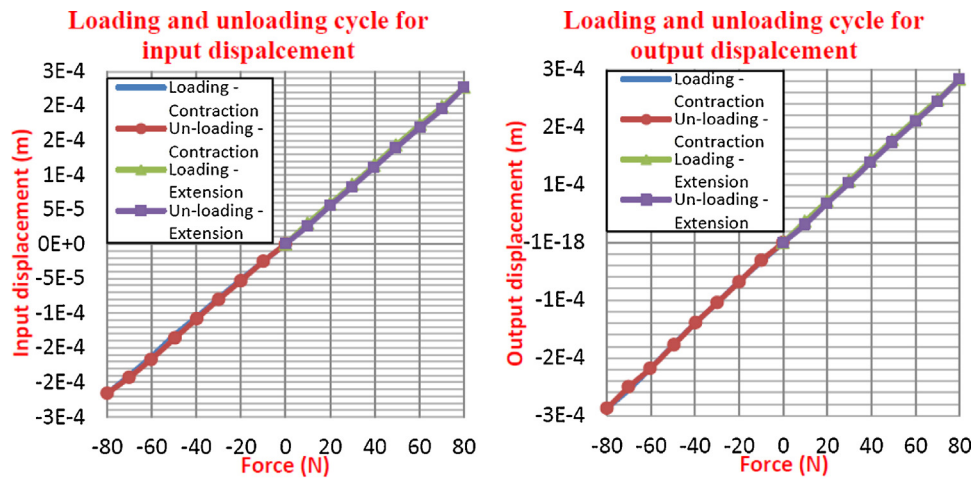
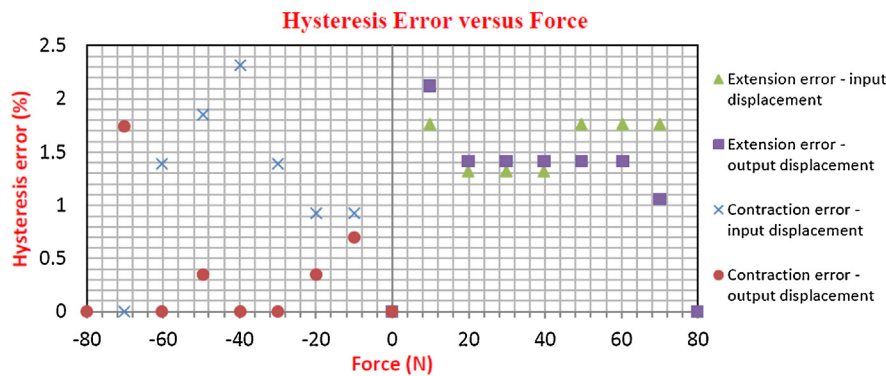


Fig. 10 – Relationship between amplification ratio and input displacement.



(a) Loading and unloading testing



(b) Hysteresis error

Fig. 11 – Hysteresis testing. (a) Loading and unloading testing. (b) Hysteresis error.

body assumption is made. In addition, the experimental results are affected by fabrication errors associated with beam thickness and corner fillet, and by loading and sensing errors.

4. Conclusions

A compact and large-range compliant gripper has been designed, modelled and bi-directionally tested in this paper. Different from these existing solutions, the proposed design stems from a 2-PRRP kinematic mechanism by using distributed-compliance joints, with the consideration of the most compact design based on a position space principle.

The testing results have shown some quantitative performance characteristics of this compliant gripper as follows:

- A nearly linear relationship between the input force/displacement and the output displacement;
- A nearly constant amplification ratio, 1.3, especially for the extension testing case (i.e., closing the jaw);
- A hysteresis error less than 2.5% for both the contraction and extension testing cases;
- A ± 0.3 mm motion range for each jaw.

The accurate analytical modelling, dynamic testing, control, and grasping testing are to be investigated following up the work in this paper. It is hoped that the miniaturised version of the compact compliant gripper can be fabricated in the near future. It is noted that the 2-PRRP mechanism can be used to design other compliant grippers when employing different compliant compositional modules with lumped and/or distributed compliance.

Acknowledgements

Mr. Tim Power and Mr. Michael O'Shea in School of Engineering at University College Cork are greatly appreciated for their excellent fabrication work of the proposed gripper.

REFERENCES

- [1] M. Nordin, P.O. Gutman, *Controlling mechanical systems with backlash – a survey*, *Automatica* 8 (10) (2002) 1633–1649.
- [2] L.L. Howell, *Compliant Mechanisms*, John Wiley & Sons, New York, 2001.

- [3] S.T. Smith, *Flexures: Elements of Elastic Mechanisms*, Gordon and Breach Science Publishers, New York, 2000.
- [4] N. Lobontiu, *Compliant Mechanisms: Design of Flexure Hinges*, CRC Press, Boca Raton, 2002.
- [5] M.N.M. Zubir, B. Shirinzadeh, Y. Tian, Development of novel hybrid flexure-based microgrippers for precision micro-object manipulation, *Review of Scientific Instruments* 80 (2009) 065106, 14 pages.
- [6] M. Goldfarb, N. Celanovic, A flexure-based gripper for small-scale manipulation, *Robotica* 17 (1999) 181–187.
- [7] S.K. Nah, Z.W. Zhong, A microgripper using piezoelectric actuation for micro-object manipulation, *Sensors and Actuators A: Physics* 133 (2007) 218–223.
- [8] J.D. Beroz, S. Awtar, M. Bedewy, T. Sameh, A.J. Hart, Compliant microgripper with parallel straight-line jaw trajectory for nanostructure manipulation, in: *Proceedings of 26th American Society of Precision Engineering Annual Meeting*, Denver, USA, 2011.
- [9] W. Ai, Q. Xu, New structural design of a compliant gripper based on the Scott-Russell mechanism, *International Journal of Advanced Robotic Systems* 11 (2014) 192, 10 pages.
- [10] Q. Xing, Design of asymmetric flexible micro-gripper mechanism based on flexure hinges, *Advances in Mechanical Engineering* 7 (6) (2015) 1–8.
- [11] M.C. Carrozza, A. Eisinberg, et al., Towards a force-controlled microgripper for assembling biomedical microdevices, *Journal of Micromechanics and Microengineering* 10 (2) (2000) 271–276.
- [12] S. Kota, K.-J. Lu, Z. Kreiner, B. Trease, J. Arenas, J. Geiger, Design and application of compliant mechanisms for surgical tools, *ASME Journal of Biomedical Engineering* 127 (2005) 981–989.
- [13] Q. Xu, Design, fabrication, and testing of an MEMS microgripper with dual-axis force sensor, *IEEE Sensors Journal* 15 (10) (2015) 6017–6026.
- [14] A.N. Reddy, N. Maheshwari, D.K. Sahu, G.K. Ananthasuresh, Miniature compliant grippers with vision-based force sensing, *IEEE Transactions on Robotics* 26 (5) (2010) 867–877.
- [15] B. Zhu, X. Zhang, N. Wang, Topology optimization of hinge-free compliant mechanisms with multiple outputs using level set method, *Structural and Multidisciplinary Optimization* 47 (5) (2013) 659–672.
- [16] Commercial PZT actuators with bridge amplification mechanisms: <http://www.cedrat.com/en/mechatronic-products/actuators/apa.html> (accessed 05.02.16).
- [17] C. Ru, L. Chen, B. Shao, W. Rong, L. Sun, A hysteresis compensation method of piezoelectric actuator: model, identification and control, *Control Engineering Practice* 17 (9) (2009) 1107–1114.
- [18] J.M. McCarthy, G.S. Soh, *Geometric Design of Linkages*, Springer-Verlag, New York, 2011.
- [19] H. Li, G. Hao, A constraint and position identification (CPI) approach for the synthesis of decoupled spatial translational compliant parallel manipulators, *Mechanism and Machine Theory* 90 (2015) 59–83.
- [20] H. Li, G. Hao, Compliant mechanism reconfiguration based on position space concept for reducing parasitic motion, in: *Proceedings of ASME 2015 International Design Engineering Technical Conferences & Computers and Information in Engineering Conference*, Boston, MA, USA, 2015.
- [21] G. Hao, H. Li, R. Kavanagh, Design of decoupled, compact, and monolithic spatial translational compliant parallel manipulators based on the position space concept, *Proceedings of the IMechE Part C: Journal of Mechanical Engineering Science* 230 (3) (2015) 367–378.
- [22] G. Hao, X. Kong, A novel large-range XY compliant parallel manipulator with enhanced out-of-plane stiffness, *Journal of Mechanical Design* 134 (2012) 061009.
- [23] G. Hao, Q. Meng, Y. Li, Design of large-range XY compliant parallel manipulators based on parasitic motion compensation, in: *Proceedings of the ASME 2013 International Design Engineering Technical Conferences & Computers and Information in Engineering Conference*, Portland, USA, 2013.